

Global and seasonal distribution of gravity wave activity in Mars' lower atmosphere derived from MGS radio occultation data

John E. Creasey and Jeffrey M. Forbes

Department of Aerospace Engineering Sciences, University of Colorado, Boulder, Colorado, USA

David P. Hinson

Department of Electrical Engineering, Stanford University, Stanford, California, USA

Received 16 July 2005; revised 14 November 2005; accepted 21 November 2005; published 4 January 2006.

[1] Temperature profiles from Mars Global Surveyor (MGS) radio occultation measurements reveal vertical wave structures assumed to be atmospheric gravity waves in Mars' lower atmosphere. For each vertical temperature profile derived from a radio occultation measurement, wave energy density is calculated, and results are locally averaged to derive a global distribution of gravity wave activity. Global distributions are determined for all values of solar longitude and for solar longitudes corresponding to northern summer and winter to show seasonality and for vertical wavelengths less than 10 km to remove the contribution from thermal tides, which dominate in the Martian tropics at larger vertical wavelengths. The global energy density patterns show significant wave activity over the tropics and the mountainous Tharsis region averaged over all seasons and enhanced activity in northern summer compared to winter. For the most part, the observed data does not correlate well with the orographic forcing schemes used to model gravity waves in general circulation models for Mars, suggesting that wave sources other than orography play an important role on Mars. **Citation:** Creasey, J. E., J. M. Forbes, and D. P. Hinson (2006), Global and seasonal distribution of gravity wave activity in Mars' lower atmosphere derived from MGS radio occultation data, *Geophys. Res. Lett.*, *33*, L01803, doi:10.1029/2005GL024037.

1. Introduction

[2] It is well established that gravity waves affect the structure and mean circulation of Earth's middle and upper atmosphere by transporting momentum and energy upward from the lower atmosphere. Sources for gravity waves include topography, near-surface thermal contrasts, wind shear instability, frontal processes, and convection. Because gravity waves grow exponentially with height, small-amplitude disturbances near the surface can have a profound effect at heights where dissipation occurs, as momentum and heat are deposited into the mean flow. Similar effects are anticipated for Mars since gravity waves are a characteristic of a stably stratified atmosphere. For example, modeling studies for Mars by *Théodore et al.* [1993], *Joshi et al.* [1995], *Collins et al.* [1997], and *Forget et al.* [1999] find that vertically-propagating gravity waves produce a force on the mean flow sufficient to close off the mid-latitude westerly jet above about 70 km and generate

significant adiabatic warming above 40–60 km in the high-latitude winter hemisphere. The effects of gravity waves are introduced into these models using a Palmer-like scheme [Palmer, 1986; Baines and Palmer, 1990] for orographic forcing, and a parameterization for wave breakdown effects based on the linear saturation scheme of Lindzen [1981].

[3] The aforementioned modeling efforts for Mars suffer from lack of observations to validate the predicted wind fields and from no experimental constraints on the gravity wave forcing. However, occultation measurements from the Mars Global Surveyor (MGS) Radio Science (RS) experiment [Hinson *et al.*, 1999] provide global measurements of temperature in Mars' atmosphere from the surface to roughly 35 km altitude, with sufficiently good vertical resolution to delineate gravity waves with vertical wavelengths between about 2.5 and 25 km. It is the purpose of this paper to provide an estimate of the global distribution of gravity wave energy fluxes in the atmosphere of Mars based on these data. Our results can form the basis for more realistic gravity wave forcing in models of Mars' middle and upper atmosphere.

2. Data Analysis

[4] From January 1998 through May 2004, MGS conducted 13,141 radio occultation soundings of the Martian neutral atmosphere, each yielding a vertical profile of temperature and pressure versus radius and geopotential extending from the surface to the 10-Pa pressure level. The method for retrieving atmospheric profiles from occultation data is discussed by Hinson *et al.* [1999]. A subset of profiles with local time between 0200 and 0600 hours was used in this study to ensure atmospheric stability within the 10–30 km height range of interest. The geographic locations of the remaining 7917 profiles are shown in Figure 1. All values of solar longitude L_s were used, with results also filtered by L_s to show seasonal variability. Interannual variations were not analyzed.

[5] For each profile, wave energy was calculated following the methods used terrestrially by Tsuda *et al.* [2000] and Eckermann *et al.* [1994] as outlined below. The approach is based on the linear theory of gravity waves such that it is possible to estimate total gravity wave energy E_0 from temperature observations only. Vertical resolution was roughly constant for each profile, but varied significantly across all profiles. Minimum, mean, and maximum vertical resolutions were 278 m, 831 m, and 1248 m respectively. To

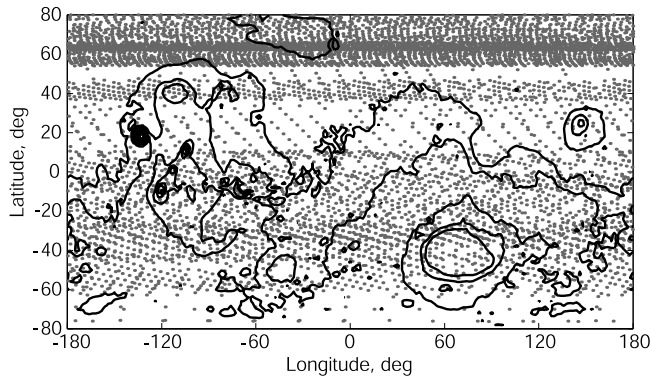


Figure 1. Distribution of radio occultation measurements relative to Martian topography. Each marker represents a vertical temperature profile derived from one radio occultation sounding.

maintain consistency in processing and simplify spectral analysis of vertical wavelength, each temperature profile was interpolated to a constant vertical grid with vertical spacing of 1250 m.

[6] The quantity used in this study as a measure of gravity wave activity is E_p , wave potential energy per unit mass, given by

$$E_p = \frac{1}{2} \left(\frac{g}{N} \right)^2 \overline{\left(\frac{T'}{T_0} \right)^2} \quad (1)$$

where g is acceleration due to gravity, N is the Brunt-Väisälä frequency, T_0 is the background temperature profile, and T' is the temperature fluctuation. All are functions of height. The background temperature profile T_0 was found for each profile by applying a least-squares third-order curve fit to the constant-grid temperature data. The temperature fluctuation T' was then determined by subtracting the background temperature from the observed temperature. Figure 2 shows two examples of MGS temperature profiles with calculated background temperatures and temperature fluctuations. Gravity wave potential energy can be related to total energy by $E_0 = E_k + E_p$ where E_k is gravity wave kinetic energy. According to the linear theory of gravity waves, the ratio of kinetic to potential energy is constant [Van Zandt, 1985], making E_0 linearly proportional to E_p . A single value of E_p for each profile was obtained by averaging E_p over a height range of 10–30 km. The lower limit was chosen to avoid the boundary layer inversion adjacent to the surface, while the upper limit was constrained to maintain data consistency across all profiles.

[7] Additionally, for each profile that showed significant activity, defined arbitrarily as a maximum temperature fluctuation greater than 1 K, the characteristic vertical wavelength was determined by taking the Fourier transform of the temperature fluctuation and then choosing the 1-km wavelength bin with the highest power.

3. Results

[8] The global distribution of gravity wave potential energy E_p in the 10–30 km height region was determined by averaging E_p values in an area 15° in latitude by the

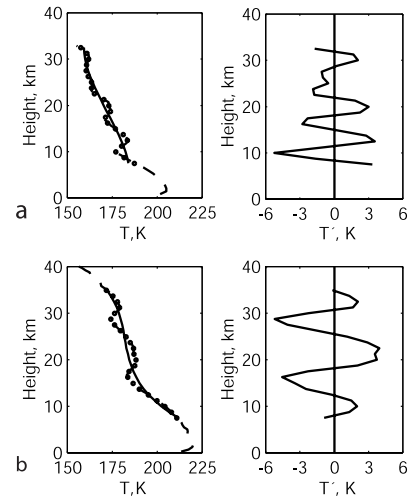


Figure 2. Selected temperature profiles (a) 9139G18A in the Tharsis region at 18°N and 113°W and (b) 9153V26A at 3°S and 160°E . In the height versus temperature plots the dashed line extending from the surface is the raw temperature data derived from the radio occultation experiment, the circles along the dashed line represent the interpolated data points with constant vertical spacing of 1250 m, and the solid line is the background temperature defined by a least-squares cubic polynomial curve fit. These profiles were selected to highlight wave activity seen in the fluctuating components with vertical wavelengths roughly (a) 6 km and (b) 12 km. Also of interest is that both profiles show evidence of wave saturation.

equatorial equivalent of 15° in longitude with the center coordinates shifted every 5° in latitude and longitude. The results reflect vertical wavelengths ranging from 2.5 km per Nyquist sampling theorem to approximately 25 km as limited by the third-order curve fit used to determine the background temperature. Figures 3 and 4 show the global distribution for all values of L_s and for northern summer and winter respectively. Distributions are not shown for northern autumn due to the limited number of profiles available

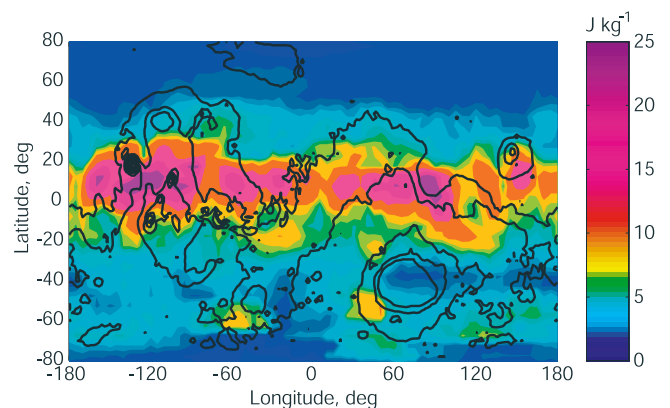


Figure 3. Global distribution of E_p , gravity wave potential energy per unit mass, at 10–30 km height for all vertical wavelengths and all values of L_s . The E_p value is averaged in an area equivalent to 15° by 15° at the equator with the center coordinates shifted every 5° .

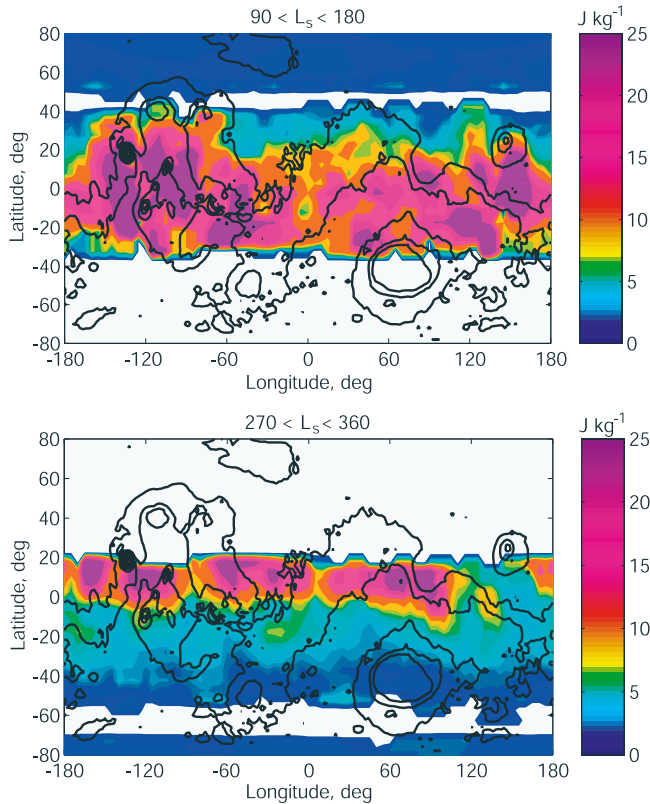


Figure 4. Global distribution of E_p , gravity wave potential energy per unit mass, at 10–30 km height for all vertical wavelengths and values of L_s corresponding to northern summer (top) and northern winter (bottom). White areas indicate regions of no data availability.

(<500) nor for northern spring because no data was available in the tropics and extra-tropical activity was consistent with Figure 3.

[9] From Figure 3, wave activity occurs predominantly in the Martian tropics, where it is distributed asymmetrically in longitude with a slight bias towards the northern hemisphere. Within the tropics, wave energy is high in the mountainous Tharsis region presumably due to topography. However, wave energy is equally high over the low-lying Isidis Planitia with elevated activity also observed in the tropics near Chryse Planitia and Amazonis Planitia. Outside the tropics, measurements reveal enhanced wave activity over the southern hemisphere extending close to the southern pole, a result expected due to the greater orographic variance in this hemisphere. Gravity waves are limited in the northern hemisphere above 50°N , though not altogether absent. Roughly 5% and 1% of all measurements taken above 50°N yielded E_p values greater than 5 J/kg and 10 J/kg respectively. These gravity waves may be further manifestations of the lee waves imaged by Mariner 9 [Briggs and Leovy, 1974]. From Figure 4, wave activity is significantly enhanced in northern summer versus winter, especially south of the equator. In northern summer, averaged wave activity in the tropics increases by a factor of 2, and the area of wave activity extends further north and south.

[10] The vertical wave activity observed in the tropics can be partly attributed to zonally modulated thermal tides

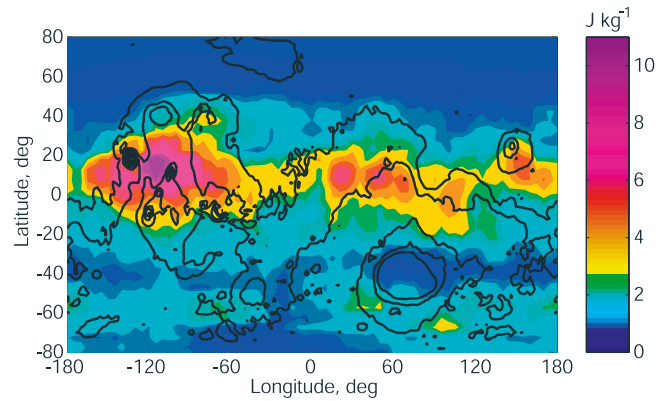


Figure 5. Global distribution of E_p , gravity wave potential energy per unit mass, at 10–30 km height for vertical wavelengths shorter than 10 km. Vertical wavelengths longer than 10 km were removed using a highpass filter. Note that the color scale has changed from Figure 3.

[Hinson and Wilson, 2004]. The thermal tides are responsible for temperature inversions which are strongest and occur most frequently over elevated terrain, particularly above Tharsis. In an effort to distinguish gravity waves from thermal tides, the characteristic vertical wavelength per profile was found using the method described earlier. The distribution of characteristic vertical wavelengths is bimodal with maxima at 8–10 km and at 13–15 km, suggesting the presence of two or more types of waves. To separate these components, each temperature fluctuation profile was highpass filtered with a cutoff wavelength at 10 km. The updated global distribution is shown in Figure 5. By excluding structures with wavelength greater than 10 km, globally averaged wave potential energy is reduced by a factor 3. In the tropics, wave activity over Isidis Planitia, Chryse Planitia, and Amazonis Planitia is significantly reduced (factor of 6 to 8), indicating that the vertical profiles are dominated by wavelengths longer than 10 km. Given the limited topography in these areas to excite gravity waves, these waves (>10 km wavelength) are likely thermal tides, although gravity waves excited by non-orographic sources

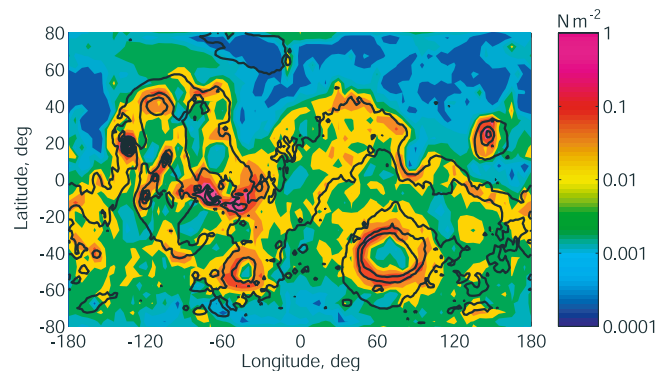


Figure 6. Stress caused by wind flow over topography. Data was calculated on a 5° grid per the resolution of the Mars Climate Database. Calculated values less than $1.0 \times 10^{-4} \text{ N m}^{-2}$ were assigned a value of 1.0×10^{-4} .

have not been ruled out. Over the Tharsis region, gravity wave activity, although reduced, is still very high.

[11] These results were compared to the predictions of general circulation models (GCMs) for Mars which use a gravity wave forcing scheme based on the surface stress, or vertical flux of momentum, caused by wind flow over topography [Forget *et al.*, 1999; Collins *et al.*, 1997]. From Palmer *et al.* [1986], the magnitude of the surface stress exerted by a vertically propagating gravity wave can be written as

$$\tau = \kappa \rho N U \sigma^2 \quad (2)$$

where ρ is atmospheric density, N is the Brunt-Väisälä frequency, U is the magnitude of the low level wind, σ^2 is the subgrid-scale orographic variance, and κ is a tunable parameter used here with a constant value of $1.0 \times 10^{-4} \text{ m}^{-1}$. Using seasonally-averaged atmospheric density and wind speed averaged over the first three levels of the Mars Climate Database [Lewis *et al.*, 1999] and orographic variance from MGS MOLA data, surface stress was calculated for all locations as shown in Figure 6. Surface stress is considerably higher in areas of significant topography, such as the Tharsis volcanoes and Elysium Mons.

[12] From the Eliassen-Palm theorem, stress is constant at all heights in the absence of transience or dissipation, and from Fritts and Van Zandt [1993], stress is linearly proportional to vertical wave energy density. Therefore, if orographic forcing was the sole source of gravity wave excitation, the distribution of surface stress in Figure 6 would more closely resemble the wave energy density distributions shown in Figures 3 and 5. Instead, gravity wave forcing on a global scale appears to be much more complex.

4. Conclusions

[13] The MGS RS experiment has greatly extended the quantity and quality of observations of gravity waves in the Martian atmosphere. Significant wave energy has been observed globally, but particularly over the Martian tropics where thermal tides may account for a large portion of the activity. Strong seasonal variations have also been observed, with wave energy in the tropics enhanced in northern summer. Gravity wave activity correlates well with topography in some cases, such as over the Tharsis region, but in some regions where topographic schemes used in Mars GCMs predict elevated wave activity, such as over Hellas Planitia, comparably little activity has been observed. The topographic schemes also fail to predict the strong peak of wave activity observed over the tropics. These results indicate that current gravity wave forcing schemes for Mars

do not sufficiently capture all disturbance sources. Further investigation is required to understand gravity wave forcing and seasonal variations, and the global distributions provided herein should serve as the observational basis.

[14] **Acknowledgment.** This work was supported by grant NNG04GJ97G from the NASA Mars Data Analysis Program to the University of Colorado.

References

- Baines, P. G., and T. N. Palmer (1990), Rationale for a new physically-based parametrization of sub-grid scale orographic effects, *Tech. Rep. 169*, Eur. Cent. for Medium-Range Weather Forecasts, Reading, U. K.
- Briggs, G. A., and C. B. Leovy (1974), Mariner 9 observations of the Mars north polar hood, *Bull. Am. Meteorol. Soc.*, *55*, 278–296.
- Collins, M., S. R. Lewis, and P. L. Read (1997), Gravity wave drag in a global circulation model of the Martian atmosphere: Parametrisation and validation, *Adv. Space. Res.*, *44*, 1395–1409.
- Eckermann, S. D., I. Hirota, and W. K. Hocking (1994), Gravity wave and equatorial wave morphology of the stratosphere derived from long-term rocket soundings, *Q. J. R. Meteorol. Soc.*, *121*, 149–186.
- Forget, F., F. Hourdin, R. Fournier, C. Hourdin, O. Talagrand, M. Collins, S. R. Lewis, P. L. Read, and J.-P. Huot (1999), Improved general circulation models of the Martian atmosphere from the surface to above 80 km, *J. Geophys. Res.*, *104*, 24,155–24,176.
- Fritts, D. C., and T. E. Van Zandt (1993), Spectral estimates of gravity wave energy and momentum fluxes, I: Energy dissipation, acceleration, and constraints, *J. Atmos. Sci.*, *47*, 51–66.
- Hinson, D. P., and R. J. Wilson (2004), Temperature inversions, thermal tides, and water ice clouds in the Martian tropics, *J. Geophys. Res.*, *109*, E01002, doi:10.1029/2003JE002129.
- Hinson, D. P., R. A. Simpson, J. D. Twicken, G. L. Tyler, and F. M. Flasar (1999), Initial results from radio occultation measurements with Mars Global Surveyor, *J. Geophys. Res.*, *104*, 26,997–27,012.
- Joshi, M. M., B. N. Lawrence, and S. R. Lewis (1995), Gravity wave drag in three-dimensional atmospheric models of Mars, *J. Geophys. Res.*, *100*, 21,235–21,245.
- Lewis, S. R., M. Collins, P. L. Read, F. Forget, F. Hourdin, R. Fournier, C. Hourdin, O. Talagrand, and J.-P. Huot (1999), A climate database for Mars, *J. Geophys. Res.*, *104*, 24,177–24,194.
- Lindzen, R. S. (1981), Turbulence and stress owing to gravity wave and tidal breakdown, *J. Geophys. Res.*, *86*, 9707–9714.
- McLandress, C. (1998), On the importance of gravity waves in the middle atmosphere and their parameterization in general circulation models, *J. Atmos. Sol. Terr. Phys.*, *60*, 1357–1383.
- Palmer, T. N., G. J. Shutts, and R. Swinbank (1986), Alleviation of a systematic westerly bias in general circulation and numerical weather prediction models through an orographic gravity wave drag parameterization, *Q. J. R. Meteorol. Soc.*, *112*, 1001–1039.
- Théodore, B., E. Lellouch, E. Chassefière, and A. Hauchecorne (1993), Solstitial temperature inversions in the Martian middle atmosphere: Observational clues and 2-D modeling, *Icarus*, *105*, 512–528.
- Tsuda, T., M. Nishida, C. Rocken, and R. H. Ware (2000), A global morphology of gravity wave activity in the stratosphere revealed by the GPS occultation data (GPS/MET), *J. Geophys. Res.*, *105*, 7257–7273.
- Van Zandt, T. E. (1985), A model for gravity wave spectra observed by Doppler sounding system, *Radio Sci.*, *20*, 1323–1330.

J. E. Creasey and J. M. Forbes, Department of Aerospace Engineering Sciences, University of Colorado, Campus Box 429, Boulder, CO 80309-0429, USA. (john.creasey@colorado.edu; forbes@colorado.edu)

D. P. Hinson, Department of Electrical Engineering, Stanford University, 350 Serra Mall, Stanford, CA 94305, USA. (dhinson@stanford.edu)